

# The Noncommutative Standard Model and Polarization in Charged Gauge Boson Production at the LHC

Thorsten Ohl<sup>\*,a</sup>  
Christian Speckner<sup>†,a,b</sup>

<sup>a</sup>Institut für Theoretische Physik und Astrophysik  
Universität Würzburg  
Am Hubland, 97074 Würzburg, Germany

<sup>b</sup>Physikalisches Institut  
Albert-Ludwigs-Universität Freiburg  
Hermann-Herder-Str. 3, 79104 Freiburg, Germany

October 29, 2010

## Abstract

We study the pair production of charged gauge bosons at the LHC in a noncommutative extension of the standard model. We use angular distributions in the decays of the gauge bosons to partially reconstruct polarized cross sections. We use this, together with  $CP$  considerations, to construct more sensitive observables that allow to separate space-time from space-space noncommutativities.

## 1 Introduction

Following the observation that Yang-Mills theories on a noncommutative (NC) spacetime represent a low energy limit of certain open string theories [1], NC gauge theories have attracted again a lot of interest. Using Seiberg-Witten Maps (SWM) [1] to map such NC gauge theories<sup>1</sup> on Yang-Mills theories living on ordinary spacetime perturbed by an infinite number of higher dimension operators in a

gauge invariant way, a consistent NC extension of the standard model (SM) to the Moyal plane has been constructed [2, 3, 4]. The Moyal plane explicitly breaks Lorentz invariance with two constant background fields  $\vec{E}$  and  $\vec{B}$  and therefore predicts dramatic new experimental signatures like the azimuthal dependence of cross sections.

A phenomenological study has been conducted for  $Z\gamma$  pair production at the Tevatron and the LHC [5] which suggests that the effects of a NC structure of spacetime should become visible at the LHC for a new physics scale  $\Lambda_{\text{NC}}$  up to 1 TeV. Since the best lower bounds on  $\Lambda_{\text{NC}}$  from collider experiments are of the order of 200 GeV, this leaves room for a discovery of noncommutativity at the LHC. The lower bound on  $\Lambda_{\text{NC}}$  could possibly be pushed to significantly higher scales by astrophysical tests as well as precision experiments from atomic physics; however, those bounds assume noncommutativity on large scales and are model dependent (for other phenomenological studies of NC extensions of the SM see [6, 7, 8]).

In this paper, we study the production of polarized  $W$  pairs at the LHC in the scenario discussed in [3] and present data generated with the Monte-Carlo eventgenerator WHIZARD [9] for this process including the semileptonic decay of the  $W$

\*e-mail: ohl@physik.uni-wuerzburg.de

†e-mail: Christian.Speckner@physik.uni-freiburg.de

<sup>1</sup>We will refer to gauge theories living on the NC manifold as “NC” gauge theories (in contrast to “commutative” gauge theories defined on ordinary spacetime), whereas the group structure will be denoted as “abelian” resp. “nonabelian”.

pair. An interesting feature of the production of  $W$  bosons is the possibility of reconstructing information about their helicity from the angular distribution of the fermionic decay products. We use this method to reconstruct the helicity distribution of the  $W$  bosons and to construct observables which in principle allow for the independent measurement of the transverse components of  $\vec{E}$  and  $\vec{B}$ .

The paper is organized as follows: in the second section we briefly review the construction of the Noncommutative Standard Model (NCSM) via the Moyal-Weyl product and the application of Seiberg-Witten maps. In the third section, we discuss the parton level cross section, with a particular emphasis on the  $CP$  properties that allow the construction of sensitive observables. In the fourth section we present results from Monte-Carlo simulations for the production of polarized  $W$  bosons in  $pp$  collisions at the LHC and construct convenient observables. In the fifth section we include the decay of the  $W$  bosons into the simulation and discuss the reconstruction of the polarized distributions from the semileptonic final state. In the appendix we correct an error in the published Feynman rules for the  $f\bar{f}W^+W^-$  vertices in the NCSM [4] and verify our result by the Ward Identities for the  $q\bar{q}W^+W^-$  amplitude in the symmetric phase.

## 2 The Noncommutative Standard Model

To construct a NC analog of Minkowski spacetime one considers four noncommuting objects  $\hat{x}^\mu$  with indices raised and lowered using the Minkowski metric  $g^{\mu\nu}$  which transform under Lorentz transformations as a four-vector. The algebra  $\hat{\mathcal{A}}$  of formal power series in the  $\hat{x}^\mu$  is then taken to be the NC equivalent of the algebra  $\mathcal{A}$  of functions (fields) on ordinary space time. It is convenient to parameterize the commutator as

$$[\hat{x}^\mu, \hat{x}^\nu] = \frac{i}{\Lambda_{\text{NC}}^2} \theta^{\mu\nu} \quad (1)$$

with the new physics scale  $\Lambda_{\text{NC}}$ . Below, we will often use the abbreviation  $\lambda = \frac{1}{\Lambda_{\text{NC}}^2}$ .

Due to its antisymmetry and transformation properties, the matrix  $\theta^{\mu\nu}$  can be parameterized

with two three-vectors  $\vec{E}$  and  $\vec{B}$

$$\theta^{\mu\nu} = \begin{pmatrix} 0 & E_x & E_y & E_z \\ -E_x & 0 & -B_z & B_y \\ -E_y & B_z & 0 & -B_x \\ -E_z & -B_y & B_x & 0 \end{pmatrix}$$

which we assume to be constant and commuting in order to obtain a Moyal plane. This implementation of noncommutativity explicitly breaks Lorentz invariance by introducing two preferred directions in space.

Instead of working directly with the elements of the algebra  $\hat{\mathcal{A}}$ , it is convenient to represent it in the algebra  $\mathcal{A}$  of ordinary fields on spacetime with the multiplication replaced by a deformed product. For the case considered here, this product is given by the Moyal-Weyl  $\star$ -product which can be written as

$$\hat{f}(x) \star \hat{g}(x) = \hat{f}(x) e^{\frac{i}{2} \lambda \overleftarrow{\partial} \theta^{\mu\nu} \overrightarrow{\partial}} \hat{g}(x) \quad (2)$$

with the arrow above a partial derivative denotes whether it is to act on  $f$  or  $g$ . The “hat” denotes functions that are to be multiplied with respect to the Moyal product. We use the notation  $a_\mu b_\nu \theta^{\mu\nu} = a\theta b$  and  $a_\mu \theta^{\mu\nu} = a\theta^\nu$  for contractions of four-vectors with the tensor  $\theta^{\mu\nu}$ .

The noncommutativity leads to complications in the construction of Yang-Mills theories, because the commutator of spacetime dependent gauge transformation does not close in the Lie algebra. This could be remedied by extending the Lie algebra to the universal enveloping algebra which also contains the anticommutators of its elements at the price of adding additional gauge degrees of freedom.

A very elegant way [2] to overcome this problem is provided by Seiberg-Witten maps [1]. SWMs are maps from the Lie algebra into the enveloping algebra

$$\tau \longrightarrow \hat{\tau}(\tau, A) \quad , \quad A^\mu \longrightarrow \hat{A}^\mu(A)$$

for the gauge parameter  $\tau = \tau_i T_i$  as well as for the gauge field  $A^\mu = A_i^\mu T_i$  such that commutative gauge transformations

$$A^\mu \xrightarrow{\tau} A^\mu_\tau$$

induce NC gauge transformations

$$\hat{A}^\mu(A) \xrightarrow{\tau} \hat{A}^\mu(A_\tau) = \hat{A}^\mu(A)_{\hat{\tau}(\tau, A)} \quad (3)$$

The gauge equivalence condition (3) can be written in infinitesimal form and, after expanding the Moyal

product in the noncommutativity parameter  $\lambda$ , the SWMs can be solved for order by order in  $\lambda$  [2]. The solution can be shown to be not unique [10]; we use the same solution as [3] which preserves the hermicity of the gauge field. These SWMs are

$$\begin{aligned}\hat{\tau}(\tau, A) &= \tau + \frac{\lambda}{4}\theta^{\mu\nu}\{\partial_\mu\tau, A_\nu\} + \mathcal{O}(\lambda^2) \\ \hat{A}^\mu(A) &= A^\mu - \frac{\lambda\theta^{\rho\sigma}}{4}\{A_\rho, \partial_\sigma A^\mu + F_\sigma{}^\mu\} + \mathcal{O}(\lambda^2)\end{aligned}$$

A similar SWM exists for the matter field  $\hat{\Psi}$  and is given by

$$\hat{\Psi}(\Psi, A) = \Psi + \frac{\lambda\theta^{\mu\nu}}{4}(iA_\mu A_\nu \Psi - 2A_\mu \partial_\nu \Psi) + \mathcal{O}(\lambda^2)$$

Inserting the SWMs into the NC Yang-Mills action

$$S = \int d^4x \hat{\mathcal{L}}_{\text{kl}} = \int d^4x \left( i\hat{\Psi} \star \hat{\not{D}} \star \hat{\Psi} - m\hat{\Psi} \star \hat{\Psi} - \frac{1}{2}\text{tr}\hat{F}^{\mu\nu} \star \hat{F}_{\mu\nu} \right) \quad (4)$$

(which is the commutative Yang-Mills action with all products replaced by  $\star$ -products) and expanding the  $\star$ -product gives a well-defined effective field theory which incorporates the noncommutativity of spacetime up to a given order in  $\lambda$ . It is gauge invariant order by order in  $\lambda$  by virtue of the gauge equivalence condition (3) and at the same time contains no new fields in addition to those already present in the commutative case. The new operators coming from the  $\lambda$ -expansion are suppressed by powers of  $\Lambda_{\text{NC}}$ . For this work, only the operators coupling two fermions to one or two gauge bosons and the operator coupling three gauge bosons are important; the corresponding Feynman rules for a generic NC Yang-Mills theory are given in  $\lambda$  in the appendix to first order.

This construction has been used to create a NC extension of the SM [3, 4]. The setup of the fermion and Higgs sectors is straightforwardly accomplished by inserting the SWM of the fields into the SM lagrangian with all products replaced by  $\star$ -products. The gauge sector comes with an ambiguity because the coupling of the gauge field components may be proportional to traces over arbitrary elements of the enveloping algebra. In contrast to the commutative case, these traces are not fixed by the

usual normalization of traces over Lie algebra bilinears, and therefore those couplings depend on the choice of representation matrices. We will work with the so-called “non-minimal” extension of the SM [3, 4] (nmNCSM). The representation of the SM  $\mathbf{SU}(3) \times \mathbf{SU}(2)_L \times \mathbf{U}(1)$  gauge group is chosen as the direct sum of the representations belonging to the fermions and the Higgs boson. The gauge field lagrangian is then written as

$$\mathcal{L}_{\text{GF}} = \text{tr} G \hat{F}^{\mu\nu} \hat{F}_{\mu\nu}$$

with the field strength given by the covariant derivative of the full product gauge group (including the gauge couplings)

$$\hat{F}^{\mu\nu} = [\hat{D}^\mu \star \hat{D}^\nu]$$

and a diagonal matrix  $G$  which is a Casimir operator of the product group.  $G$  is parameterized by six constants  $\frac{1}{g_1^2}, \dots, \frac{1}{g_6^2}$  and enforces the correct trace over bilinears of group generators. This condition leaves three free parameters which are further constrained to the intersection of simplices [7] by the condition  $\frac{1}{g_i^2} \geq 0$  which ensures of the positivity of the hamiltonian [11]. Only one of those three parameters enters the vertices relevant for this work; in accordance with [7], we parameterize it as

$$\kappa_2 = \frac{1}{4} \left( \frac{1}{g_5^2} + \frac{1}{g_6^2} - \frac{1}{g_2^2} \right)$$

Plugging the SM couplings into the consistency equations for the  $g_i^2$  and putting no further constraints on them, the simplex condition for  $\kappa_2$  reduces to

$$-\frac{1}{4g^2} \leq \kappa_2 \leq \frac{1}{4g^2} \quad (5)$$

where  $g$  is the isospin gauge coupling.

We will neglect all corrections to the couplings between massive fields and gauge fields induced by the SWM for the Higgs field. All other Feynman rules relevant for this work are collected to first order in  $\lambda$  in the appendix.

### 3 Parton Level Analysis

In this section we analyze in detail the partonic process  $\bar{d}d \rightarrow W^+W^-$  in the NCSM, while the identical discussion for  $\bar{u}u \rightarrow W^+W^-$  does not need to

be repeated. The scattering amplitude is expanded in  $\lambda$

$$\mathcal{M} = \mathcal{M}_0 + \lambda \mathcal{M}_1 + \mathcal{O}(\lambda^2)$$

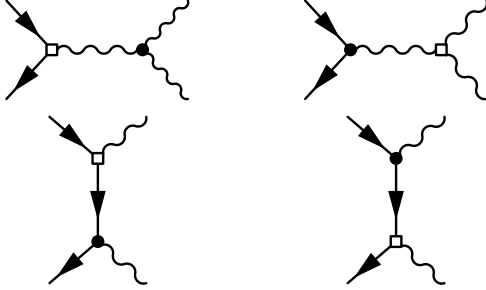
and we study the effects of the NC corrections only to first order in  $\lambda$ .

For calculating the squared matrix element  $|\mathcal{M}|^2$ , higher orders should also be truncated to keep the expansion consistent, leading to

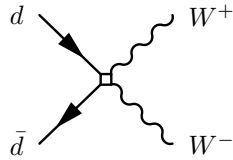
$$|\mathcal{M}|^2 = |\mathcal{M}_0|^2 + 2\lambda \Re \mathcal{M}_0 \mathcal{M}_1^* + \mathcal{O}(\lambda^2) \quad (6)$$

In principle, this truncation might yield negative cross sections in some regions of phase space. There the NC contribution dominates over the SM amplitude and the inclusion of higher orders in  $\lambda$  is necessary to keep the expansion positive [12]. However, while being a more serious problem at small  $\Lambda_{\text{NC}}$  and/or high  $q\bar{q}$  invariant mass  $\sqrt{s}$  [5, 12], this contribution turns out to be very small and can be safely ignored for the range of  $\Lambda_{\text{NC}}$  and  $\sqrt{s}$  discussed in this work.

At order  $\mathcal{O}(\lambda^0)$ , there are two  $s$  channel diagrams and one  $t$  channel diagram contributing to this process. At  $\mathcal{O}(\lambda^1)$ , each of these diagrams receives two corrections that are obtained by replacing one of the vertices by its  $\mathcal{O}(\lambda^1)$  correction<sup>2</sup>:



In addition, there is a new contact-type diagram which is not present in the SM:



In the absence of electroweak symmetry breaking, gauge symmetry forces the Feynman amplitude to

<sup>2</sup>We denote SM vertices with filled dots and the NC corrections with empty squares.

satisfy the Ward identity at all orders in  $\lambda$ , specifically at first order, e.g.:

$$\mathcal{M}_{1\mu\nu}(k_1, k_2) \epsilon_1^\mu(k_1) k_2^\nu = 0$$

In appendix B, we have checked that this explicitly. Notably, the  $\mathcal{O}(\lambda^1)$  corrections coming from the vertices coupling three gauge bosons vanish independently of the other diagrams. This is due to these vertices depending on the group representation chosen for the gauge sector, which does not influence the other vertices. Also, the  $s$ - and  $t$ -channel contributions don't cancel completely; the new contact diagram is necessary for gauge invariance.

In this section, we analyze the process in the center of mass system (CMS). We label the three-momentum of the  $d$  as  $\vec{p}$  and that of the  $W^-$  as  $\vec{k}$ , with  $\vec{p}$  oriented in positive  $x_3$ -direction.

As the introduction of the tensor  $\theta^{\mu\nu}$  explicitly breaks Lorentz invariance, a dependence of the cross section on the azimuthal angle can be expected to arise. If the external particles are in helicity eigenstates, the cross section is symmetric under simultaneous rotations of  $\vec{k}$  and the NC vectors  $\vec{E}$  and  $\vec{B}$  around the  $x_3$ -axis; therefore, rotating  $\vec{k}$  by  $\phi$  has the same effect as rotating the NC vectors by  $-\phi$ . Because the expansion of the cross section is truncated after the first order in  $\lambda$  and only contains terms at most linear in the  $E_i$  and  $B_i$ , the dependence on the azimuthal angle  $\phi$  must therefore be a harmonic oscillation with period  $2\pi$ . By virtue of the same rotational covariance, corrections proportional to  $E_3$  and  $B_3$  must be independent of  $\phi$ .

In the SM, CP symmetry forces the quark spin summed CMS cross section to be invariant under simultaneous interchange and reversal of the  $W$  helicities

$$(h_+, h_-) \xrightarrow{\text{CP}} (-h_-, -h_+) \quad (7)$$

with  $h_\pm \in \{-1, 0, +1\}$  denoting the  $W^\pm$  helicities. The P transformation properties of the commutative gauge theory carry over to the NC counterpart if  $\vec{E}$  transforms as a vector and  $\vec{B}$  as a pseudovector. However, for the C transformation properties to carry over, an appropriate choice of SWMs (the maps used in this work satisfy this) and a transformation of  $\theta^{\mu\nu}$  is necessary [11, 13]

$$\theta^{\mu\nu} \xrightarrow{\text{C}} -\theta^{\mu\nu}$$

This CP covariance implies that the NCSM CMS cross section is invariant under the replacement

$$\left. \begin{pmatrix} h_+, h_- \\ \vec{E} \\ \vec{B} \end{pmatrix} \right\} \xrightarrow{\text{CP}} \left\{ \begin{pmatrix} -h_-, -h_+ \\ \vec{E} \\ -\vec{B} \end{pmatrix} \right. \quad (8)$$

or, adopting a different point of view, that the CMS cross sections linked by (7) must differ by the sign of  $\vec{B}$ . Since cross sections to first order in  $\lambda$  can depend at most linearly on  $\vec{B}$ , the dependence on  $\vec{B}$  must cancel in that order after summing over the helicities.

We have calculated the analytical expression for the squared matrix element summed over helicities and spins using FORM [14] (with the simplification of vanishing  $Z$  width). The result can be put into the form

$$|\mathcal{M}|^2 = M_0 + \lambda \vec{E} \left( \vec{k} \times \vec{p} \right) M_1 + \mathcal{O}(\lambda^2) \quad (9)$$

where  $M_0$  and  $M_1$  are independent of  $\phi$ . As argued above, (9) is independent of  $\vec{B}$ . In the chosen frame of reference, this can also be written as

$$|\mathcal{M}|^2 = M_0 + \frac{1}{\Lambda_{\text{NC}}^2} \frac{\sqrt{s}}{2} |\vec{k}| \sin \theta \cdot (E_1 \sin \phi - E_2 \cos \phi) M_1 + \mathcal{O}(\lambda^2) \quad (10)$$

(with the mandelstam  $s$ ) making explicit the harmonic dependence on  $\phi$ . (10) shows that the squared amplitude is also independent of the longitudinal component of  $\vec{E}$ . We have checked the gauge invariance of our result by analytically testing the Ward identities for vanishing  $Z$  and  $W$  mass.

Fig.1 shows the NC corrections to the differential cross section  $\frac{d\sigma}{d\cos\theta d\phi}$  for  $\sqrt{s} = 500$  GeV,  $\Lambda_{\text{NC}} = 500$  GeV and  $\vec{E} = (1, 0, 0)^T$ . Equation (10) shows that for this choice of  $\vec{E}$  the extrema of the azimuthal oscillation are located at  $\phi = \pm \frac{\pi}{2}$ , so the plot displays the maximal deviation of the NCSM cross section from the SM prediction. The deviation has two maxima with a relative deviation of  $\approx 20\%$  and  $\approx 120\%$ ; however, at these points the differential cross section differs from its maximum by several orders of magnitude. In the vicinity of the maximum at  $\cos\theta = 1$  the deviation is only of the order  $< 5\%$ . Despite  $\kappa_2$  being chosen near the limit of the allowed interval (5), the plot shows that the correction proportional to  $\kappa_2$  is much smaller than

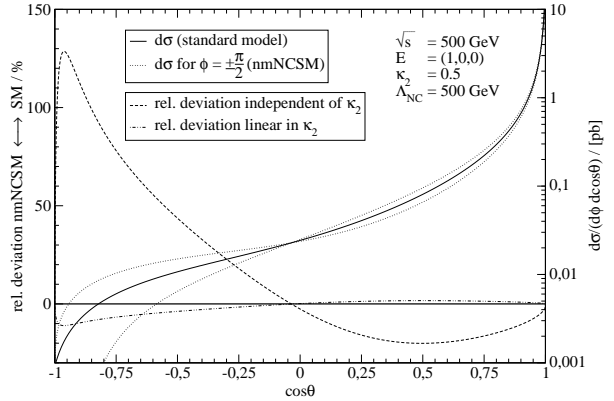


Figure 1: Maximal deviation of  $\frac{d\sigma}{d\cos\theta d\phi}$  summed over spins and helicities for the process  $d\bar{d} \rightarrow W^+W^-$ .

that independent of  $\kappa_2$ . This can be understood by noting that the new parameter only appears in the  $s$ -channel diagrams, whereas the cross section is dominated by the  $t$ -channel diagram for CMS energies high compared with the  $W$  mass. Therefore, we will ignore the effect of  $\kappa_2$  for the remainder of this paper.

We have also implemented the NC vertices and diagrams into a FORTRAN 90 module which we combined with code generated by the matrix element generator O'Mega [15] to calculate the cross section for the production of polarized  $W$  pairs numerically. Again, we have performed a (numerical) check of the Ward identities in the limit of vanishing  $W$  and  $Z$  masses; we have also checked that the cross section matches the analytical result after helicity summation.

As a consequence of the finite  $Z$  width taken into account in the numerical calculation, the cross section exhibits a small dependence on the longitudinal component of  $\vec{E}$ . Because this correction is smaller than 0.01% of the SM cross section for reasonable values of the NC parameters, it seems to be of little experimental relevance.

Turning to the polarized cross sections, we find a dependence on the longitudinal part of  $\vec{B}$  proportional to  $\kappa_2$  if the final state consists a longitudinal and a transverse gauge boson. However, the dominant combination of helicities for  $d\bar{d} \rightarrow W^+W^-$  is  $(+, -)$  (in contrast, for  $u\bar{u} \rightarrow W^+W^-$  it is  $(-, +)$ ) and all other combinations are suppressed by at

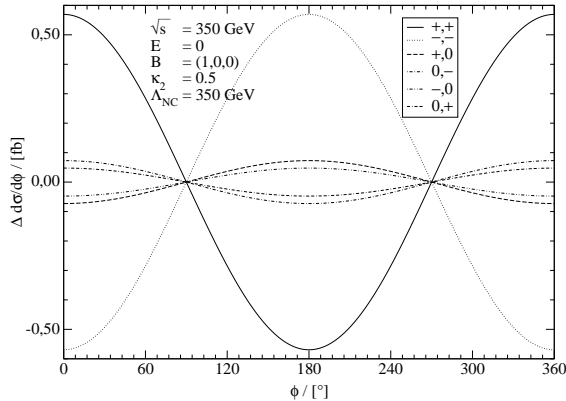


Figure 2: Azimuthal oscillation proportional to  $\vec{B}$  of the differential cross section integrated over  $\cos \theta$ .

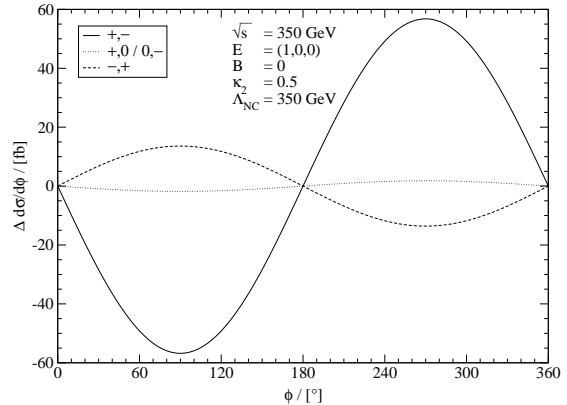


Figure 3: Azimuthal oscillations proportional to  $\vec{E}$  of the differential cross section integrated over  $\cos \theta$ .

least one order of magnitude for  $\sqrt{s} > 300$  GeV. Therefore, this effect is only a small shift in a already suppressed quantity and is unlikely to be observable in collider experiments. The remaining observable is the azimuthal oscillation of the cross section.

Fig.2 shows the dependence of  $d\sigma$  integrated<sup>3</sup> over  $\cos \theta$  on  $\phi$  for all combinations of helicities for which an azimuthal oscillation proportional to  $\vec{B}$  is allowed at  $\mathcal{O}(\lambda^1)$  by CP covariance (8). This covariance is clearly visible and causes the oscillation to cancel out in the helicity sum. In addition, the oscillation vanishes for final states containing a longitudinal gauge boson if  $\kappa_2$  is set to zero. Although the oscillation is clearly visible in the plots, the cross section is strongly suppressed for these combinations of helicities. Therefore, these channels will be very challenging to investigate at a collider in the near future.

Fig.3 shows the azimuthal oscillation proportional to  $\vec{E}$  (combinations for which the oscillation is barely visible at the chosen scale have been omitted from the plot). Again, the CP covariance is evident, in this case forcing the cross sections for final states linked by (7) to be identical. In addition, the plot reveals a partial cancellation in the helicity sum between the azimuthal oscillation for the combinations  $(+, -)$  and  $(-, +)$  which reduces the oscillation exhibited by the summed cross section.

<sup>3</sup>Choosing a different integration interval does not significantly enhance the observed oscillation as  $d\sigma$  has a sharp peak at  $\cos \theta = 1$ .

Therefore, information about the helicity distribution of the  $W$ -bosons should improve observables that probe for NC extensions of the SM in this process.

## 4 Pair Production at the LHC

We have used the Monte-Carlo eventgenerator WHIZARD [9] together with custom FORTRAN code to simulate the process  $pp \rightarrow W^+W^-$  at the LHC. A possible problem that haunts this approach is the truncation of the cross section at order  $\mathcal{O}(\lambda^1)$  (6) which causes  $d\sigma$  to assume negative values in some (suppressed) regions of phase space as discussed above. The Monte-Carlo code cannot handle this and therefore the adaption process does not converge. We have chosen to follow [5] and circumvent this by replacing the differential cross section  $d\sigma$  with

$$\max\{d\sigma, 0\}$$

which is supported by second order calculations [12]. We have used the CTEQ5M [16] series of PDFs with a running factorization scale equal to  $\sqrt{s}$ . The eventgenerator keeps track of the helicities of the  $W$  bosons; we used this information to discriminate between the  $W$  helicities in the analysis presented in this section.

We generated  $1.5 \cdot 10^6$  events (which corresponds to an integrated luminosity of  $\int dt \mathcal{L} \approx 20 \text{ fb}^{-1}$ ) with a hadronic CMS energy of 14 TeV in each run

and applied a cut

$$200 \text{ GeV} \leq \sqrt{s} \leq 1 \text{ TeV} \quad (11)$$

that removes events near the production threshold (which are supposedly more contaminated with background processes) as well as events with very high CMS energy (for which the cancellation of the expansion at  $\mathcal{O}(\lambda^1)$  may not be justified). Since any acceptance cuts on the polar angle don't affect the  $W$ -momenta directly but rather those of the decay products, we didn't apply any such cuts.

As the partonic initial states contain one valence quark (the quark) and one sea quark (the antiquark), the partonic CMS system generally is strongly boosted with respect to the laboratory system. This boost mixes the transversal components of the NC vectors according to

$$\begin{aligned} E_1 &\xrightarrow{\Lambda} \gamma(E_1 - \beta B_2) & B_1 &\xrightarrow{\Lambda} \gamma(B_1 + \beta E_2) \\ E_2 &\xrightarrow{\Lambda} \gamma(E_2 + \beta B_1) & B_2 &\xrightarrow{\Lambda} \gamma(B_2 - \beta E_1) \end{aligned}$$

(with the usual Lorentz factors  $\beta$  and  $\gamma$ ) and also mixes the polarization vectors. As a result,  $\vec{B}$  in the laboratory frame gets mapped to  $\vec{E}$  in the CMS and therefore its influence on the cross section may be much greater than the CMS result of the last section suggests.

The initial state contains two identical particles, and therefore the azimuthal distribution must be invariant under rotations by  $\pi$  around the  $x_1$  and  $x_2$  axes if no asymmetric polar cuts are made (again simultaneously rotating  $\vec{E}$  and  $\vec{B}$ ). This means invariance under the replacements

$$E_1 \rightarrow -E_1 \quad B_1 \rightarrow -B_1 \quad \phi \rightarrow \pi - \phi$$

as well as

$$E_2 \rightarrow -E_2 \quad B_2 \rightarrow -B_2 \quad \phi \rightarrow -\phi$$

implying that any observable azimuthal oscillation caused by  $E_1$  and  $B_1$  must be proportional to  $\cos \phi$ , while parts proportional to  $\sin \phi$  must cancel between events with antiquarks coming from negative  $x_3$  direction and those with antiquarks coming from positive  $x_3$  direction. Therefore, as Fig.3 shows that the oscillation caused by  $E_1$  is proportional to  $\sin \phi$ , one would expect it to cancel out, while  $B_1$  (getting mapped to  $E_2$ ) should cause an oscillation proportional to  $\cos \phi$ .

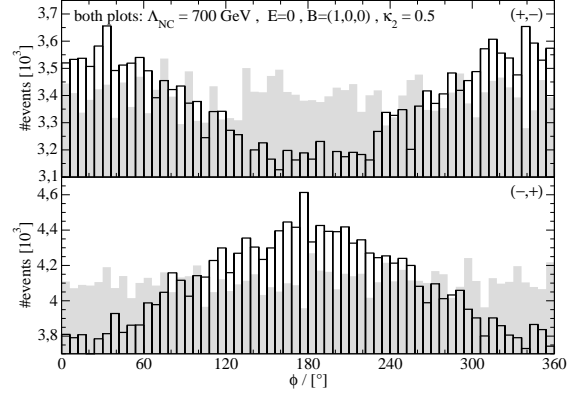


Figure 4: Oscillation of the azimuthal distribution proportional to  $\vec{B}_\perp$ ; no cuts on the polar angle.

Examining the azimuthal distributions without cuts on the polar angle  $\theta$ , one does indeed find such an oscillation proportional to  $\vec{B}_\perp$ , but none proportional to  $\vec{E}_\perp$ . To observe such an effect, one has to apply appropriate cuts that favor antiparticles coming from either positive or negative  $x_3$  direction [5]. One can easily convince oneself that the cut

$$0 \leq (\theta_- + \theta_+) \leq \pi \quad (12)$$

favors events with antiquark momenta pointing in negative  $x_3$  direction, while the complementary cut

$$\pi \leq (\theta_- + \theta_+) \leq 2\pi \quad (13)$$

favors the opposite case.

Fig.4 shows the azimuthal distribution for  $\Lambda_{\text{NC}} = 700 \text{ GeV}$  compared with the SM prediction for the helicity combinations  $(-, +)$  and  $(+, -)$  and  $\vec{B} = (1, 0, 0)^T$ ,  $\vec{E} = 0$ . All Monte-Carlo distributions show the azimuthal angle of the  $W^-$  (that of the  $W^+$  differs just by a shift of  $\pi$ ). The gray distributions are the SM expectation. Both distributions exhibit a significant oscillation with a relative phase shift of  $\pi$ ; the total event count is larger for the combination  $(-, +)$ . The azimuthal distribution for the case of  $\vec{B} = 0$ ,  $\vec{E} = (1, 0, 0)^T$  after application of cut (12) is displayed in Fig.5. Again, a rather large oscillation can be observed with a phase shift of  $\pi$  between  $(-, +)$  and  $(+, -)$ . This oscillation is *not* visible if no asymmetric cuts on the polar angle are applied.

There is a similar azimuthal oscillation proportional to  $\vec{E}_\perp$  and  $\vec{B}_\perp$  for the combination  $(-, -)$ ;

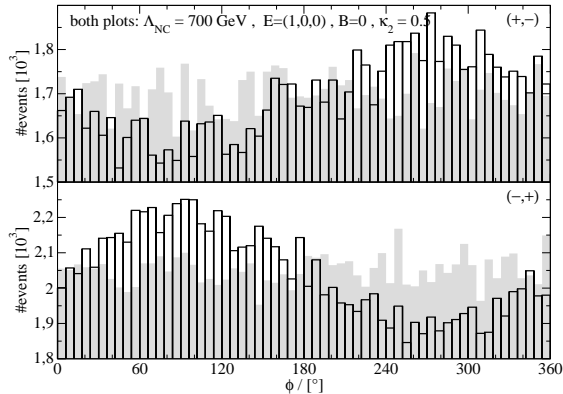


Figure 5: Oscillation of the azimuthal distribution proportional to  $\vec{E}_\perp$  after applying cut (12).

however, the statistics is much lower for this combination of helicities. Finally, there are no visible oscillations for  $(+, +)$  and the SM cross section is much smaller for this combination anyway. The simulated distributions show no visible dependence on the longitudinal components of the NC vectors which is consistent with the fact of those contributions to the partonic cross section being very small (the longitudinal components of  $\vec{E}$  and  $\vec{B}$  are not affected by the boost from the laboratory frame into the CMS).

Since the azimuthal oscillation proportional to  $\vec{E}_\perp$  cancels out if no cut on  $\theta$  is applied, the oscillations for the two cuts (12) and (13) must differ only by a phase shift of  $\pi$  causing them to cancel out in the sum. Therefore, taking those two distributions, shifting one of them by  $\pi$  and then summing them up will cause the oscillations proportional to  $\vec{E}_\perp$  to add up constructively and increase the statistics by a factor of two. In addition, the simulations show that the oscillation proportional to  $\vec{B}_\perp$  is the same for the cuts (12) and (13) and therefore cancels in this sum. This way, at first order in  $\lambda$ , measuring the azimuthal distribution without any (or with symmetric) cuts on  $\theta$  in principle allows for the determination of  $\vec{B}_\perp$ , while measuring the azimuthal distributions for the cuts (12), (13) and adding them with a shift of  $\pi$  filters out the oscillation proportional to  $\vec{B}_\perp$  and allows for an independent measurement of  $\vec{E}_\perp$ .

Note that our results differ from those presented in [17], which predicts a stronger dependence on  $\vec{E}_\perp$

effect at the LHC. We can reproduce the numbers of [17] using the  $f\bar{f}W^+W^-$  Feynman rule (85) in [4] both for  $u\bar{u}W^+W^-$  and for  $d\bar{d}W^+W^-$  vertices. However, the correct vertices in appendix A.2 have different momentum dependences. We prove this in appendix B by checking the Ward Identities for  $q\bar{q}W^+W^-$  in the symmetric phase.

## 5 Semileptonic Decay and Helicity Reconstruction

In order to apply the observables constructed in the last section to real measurements at the LHC, we must account for the fact that  $W$  bosons are unstable and decay. Specifically, we will concentrate on the semileptonic decay channel  $pp \rightarrow W^+W^- \rightarrow e\bar{\nu}_e u\bar{d}$ .

In the narrow width approximation, integrating over the azimuthal angles of the fermionic decay products (with the momentum of the parent  $W$  boson as polar axis), the cross section decomposes as

$$\frac{d\sigma}{d^3k_+ d^3k_- d\theta_+ d\theta_-} \propto \sum_{h_+h_-} \frac{d\sigma_{h_+h_-}}{d^3k_+ d^3k_-} P_{h_+}(\cos\bar{\theta}_+) P_{h_-}(\cos\bar{\theta}_-)$$

where the  $k_\pm$  are the four-momenta of the intermediary  $W$  bosons,  $\bar{\theta}_\pm$  are the polar angles of the  $\bar{\nu}_e$  resp.  $\bar{d}$  in the CMS of the  $W$ s,  $d\sigma_{h_+h_-}$  is the cross section for the production of polarized  $W$  bosons and the  $P_h$  are polynomials

$$P_h(x) = \begin{cases} \frac{1}{2}(1 \pm x)^2 & \text{for } h = \pm 1 \\ 1 - x^2 & \text{for } h = 0 \end{cases}$$

The functions

$$Q_h(x) = \begin{cases} -\frac{1}{2} \pm x + \frac{5}{2}x^2 & \text{for } h = \pm 1 \\ 2 - 5x^2 & \text{for } h = 0 \end{cases}$$

have the projection property

$$\int_{-1}^1 dx Q_h(x) P_{h'}(x) = \delta_{hh'} \int_{-1}^1 dx P_{h'}(x)$$

Therefore, it is possible to obtain the cross section for the production of polarized  $W$  bosons by convoluting the cross section for  $pp \rightarrow W^+W^- \rightarrow e\bar{\nu}_e u\bar{d}$



with the  $Q_r$ , projecting out the contribution of a certain helicity combination to the cross section. On the level of counting events, this can be done by binning the events with weights

$$w_{h_+h_-} = Q_{h_+}(\cos\bar{\theta}_+) Q_{h_-}(\cos\bar{\theta}_-)$$

The resulting distributions of the weighted events then reproduce the pair production distributions for the helicity combination  $(h_+, h_-)$ , and summing over the helicity indices reproduces the unweighted distributions by virtue of the normalization of the  $Q_h$ .

However, measuring the charge of a quark jet is virtually impossible, and therefore the corresponding angle  $\bar{\theta}$  can only be measured up to a sign. Since  $Q_0(x) = Q_0(-x)$  and  $Q_{\pm 1}(-x) = Q_{\mp 1}(x)$ , this boils down to not being able to discriminate between the transverse polarizations of the hadronically decaying  $W$ .

If the number of events in a bin  $N(k_i^\pm, x_i^+, x_j^-)$  (with the abbreviation  $x^\pm$  for  $\cos\bar{\theta}_\pm$ ) is distributed with a statistical error  $\Delta N = \sqrt{N}$ , then the statistical error  $\Delta N_{h_+h_-}$  of the corresponding bin  $N_{h_+h_-}$  in the reconstructed distribution is given by the geometric mean

$$\Delta N(k_l^\pm)_{h_+h_-} = \sqrt{\sum_{ij} N(k_l^\pm, x_i^+, x_j^-) Q_r(x_i^+)^2 Q_s(x_j^-)^2} \quad (14)$$

where the sum runs over some division of the allowed range of  $\cos\bar{\theta}_\pm$  (or over single events). Explicit calculation shows

$$\int_{-1}^1 dx P_h(x) Q_{h'}(x)^2 > \int_{-1}^1 dx P_h(x) Q_{h'}(x)$$

for all  $h, h'$  and therefore the statistical error of the reconstructed distribution will be greater than  $\sqrt{N_{h_+h_-}}$ .

As the neutrino coming from the leptonically decaying  $W$  cannot be detected directly, its momentum has to be reconstructed from the other momenta and  $p_{T,\text{miss}}$ . This can be done using the mass shell conditions of the  $W$  and that of the neutrino; see [18] for more details. However, this procedure gives two solutions for neutrino momentum, one of which approximates the correct momentum for events that can be assigned to a decaying  $W$ .

There is no simple way to discriminate between those two solutions; the simulated data shows that one has in fact to choose between them on a per event basis to get a reasonable reconstruction of the neutrino momentum. We have found that choosing the solution that minimizes the cosine of the angle between the two  $W$  momenta allows to reconstruct at least 60% of the momenta correctly. By a “correctly” reconstructed momentum we mean the solution with  $p^3$  being closest to the “truth” neutrino momentum available from Monte-Carlo data. Also, simulation shows that this method of choosing solutions preserves the oscillations discussed in the last section and still allows for the independent measurement of  $\vec{E}_\perp$  and  $\vec{B}_\perp$  (this is nontrivial since incorrectly reconstructed events might mix up the complementary distributions that combine to cancel out the oscillations proportional to  $\vec{E}_\perp$  resp.  $\vec{B}_\perp$ ). Therefore, we have chosen to use this criterion to disambiguate the two solutions in our analysis<sup>4</sup>.

In addition to the cascade diagrams, there are 17 additional SM diagrams contributing to the matrix element for  $d\bar{d} \rightarrow e\bar{\nu}_e u\bar{d}$  and similarly for  $u\bar{u} \rightarrow e\bar{\nu}_e u\bar{d}$ . These background diagrams contain one separate gauge equivalence class [19] which consists of all diagrams with one quark line connecting initial and final states and which we chose to ignore as these topologies can be strongly suppressed with invariant mass cuts. As the other diagrams are necessary for gauge invariance, we have implemented them together with the cascade type diagrams into an event generator using WHIZARD.

We have generated events for an integrated luminosity of  $\int dt \mathcal{L} = 400 \text{ fb}^{-1}$  and have also included the cases of the quark pair being  $c\bar{s}$  and the lepton-neutrino pair being one of  $\mu^- \bar{\nu}_\mu$ ,  $\tau^- \bar{\nu}_\tau$  with a naive factor of 6 on the integrated luminosity<sup>5</sup>.

In addition to the cut (11) on  $\sqrt{s}$  we also applied an acceptance cut

$$5^\circ \leq \theta \leq 175^\circ \quad (15)$$

to all particle momenta (with the exception of the neutrino momentum) and a cut

$$70 \text{ GeV} \leq m_+ \leq 90 \text{ GeV}$$

<sup>4</sup>Another possibility of dealing with the two solutions would be to count them both into the histogram like in [18], obtaining better signal statistics at the price of more noise.

<sup>5</sup>Statistics can be improved by an additional factor 2 if semileptonic decays of the type  $pp \rightarrow e^+ \nu_e \bar{u} d$  are also included.

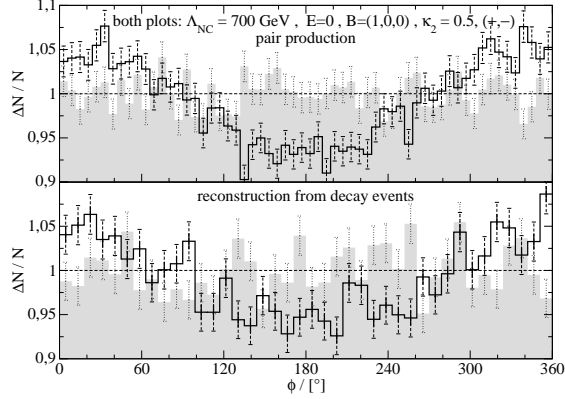


Figure 6: Comparison of the azimuthal distribution of  $1.5 \cdot 10^6$  simulated events for  $W$  pair production with that of events reconstructed from the simulation of  $pp \rightarrow e\bar{\nu}_e u\bar{d}$  ( $\approx 3.7 \cdot 10^6$  events).

on the invariant mass of the jet (quark) pair.

Fig.6 shows an azimuthal distribution obtained from the simulated production of polarized  $W$  pairs versus the corresponding distribution obtained after reconstructing the helicity distribution from the semileptonic decay (the neutrino momentum has been directly extracted from Monte-Carlo data for this distribution). In the first case, the error bars have been calculated as  $\sqrt{N}$ , in the second case according to (14). Although the statistics is much better for the second case ( $\approx 3.7 \cdot 10^6$  events in contrast to  $1.5 \cdot 10^6$ ) and the number of bins has been reduced from 60 to 40, the statistical error is of the same order than that in the first case. This fact is further emphasized by the thick black error bars in the second distribution which show the errors to be expected if the events were distributed as  $\sqrt{N}$  and which are much smaller than the actual fluctuations.

As stated above, it is not possible to discriminate between the transverse polarizations of the hadronically decaying  $W^+$ , so we sum over both, denoting the sum of distributions for the helicities  $(+, -)$  and  $(+, +)$  as  $(+, \mp)$  and the sum of  $(-, +)$  and  $(-, -)$  as  $(-, \pm)$ . The distributions Fig.4 and Fig.5 show that the relative oscillations for  $(+, -)$  and  $(-, +)$  differ only by a shift of  $\pi$ , so we can enhance the observables further by shifting the azimuthal distribution for  $(-, \pm)$  by a phase of  $\pi$  and adding it to that for  $(+, \mp)$ .

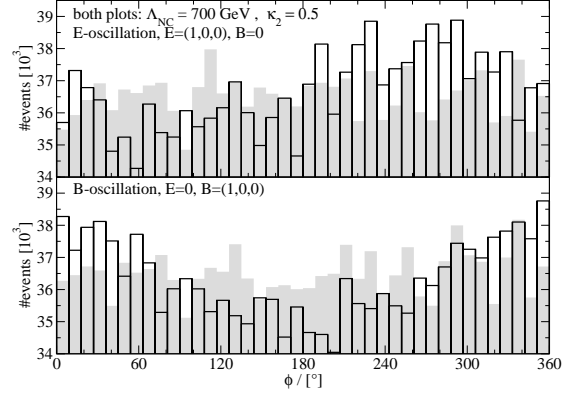


Figure 7: Azimuthal oscillations at the LHC after reconstruction of the momenta and the helicity distributions for  $\Lambda_{\text{NC}} = 700 \text{ GeV}$ ;  $\int dt \mathcal{L} = 400 \text{ fb}^{-1}$ .

To put together all the steps in our final analysis: we reconstruct the neutrino momenta and bin the events weighted with the projector functions to obtain azimuthal distributions for the production of polarized  $W$  bosons. Adding the distributions for  $(+, \mp)$  and  $(-, \pm)$  with a phase shift of  $\pi$  and without any polar cuts apart from (15), we obtain an observable which is sensitive only to  $\vec{B}_\perp$  and *not* to  $\vec{E}$ , the oscillation of which we will call  $\vec{B}$ -oscillation. Taking the same sum for each of the two cuts (12) and (13) and adding those distributions with a phase shift of  $\pi$ , we obtain another observable which is sensitive to  $\vec{E}_\perp$  only, the oscillation of which we will call  $\vec{E}$ -oscillation. The phase of these oscillations can be used to determine the alignment of  $\vec{E}_\perp$  and  $\vec{B}_\perp$  in the plane perpendicular to the beam axis, while their magnitude contains information about the absolute values.

Fig.7 and Fig.8 show these observables for  $\Lambda_{\text{NC}} = 700 \text{ GeV}$  and  $\Lambda_{\text{NC}} = 1 \text{ TeV}$ . For  $\Lambda_{\text{NC}} = 700 \text{ GeV}$ , the azimuthal oscillation is clearly visible, although comparison with Fig.4 and Fig.5 shows that the statistical error of the distribution is much larger than for the hypothetical case of  $W$  pair production (even though we simulated  $\approx 3.7 \cdot 10^6$  events as opposed to the  $1.5 \cdot 10^6$  events in the pair production simulation). For  $\Lambda_{\text{NC}} = 1 \text{ TeV}$ , the oscillation is still visible.

To get a quantitative handle on the significance of the oscillations, we have done a naive calculation of  $\chi^2$  with respect to the SM prediction for the his-

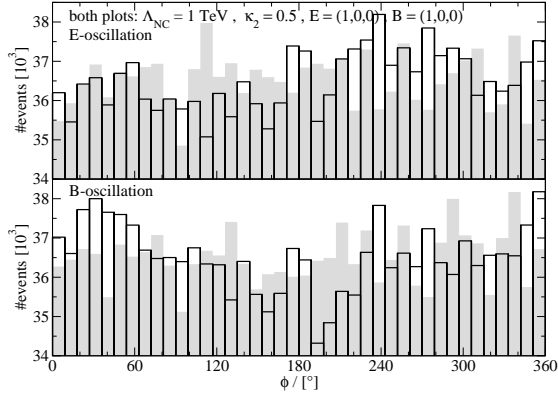


Figure 8: Like Fig.8 for  $\Lambda_{\text{NC}} = 1 \text{ TeV}$ .

tograms Fig.7 and Fig.8. For  $\Lambda_{\text{NC}} = 700 \text{ GeV}$ , this shows a clear deviation from the standard model. Unfortunately, for  $\Lambda_{\text{NC}} = 1 \text{ TeV}$ , this naive  $\chi^2$  test shows no clear deviation from the SM, suggesting 1 TeV might be the limit of the LHC discovery reach in this channel (consistent with the results obtained in [5]). The analysis might be improved over the  $\chi^2$  test by considering a quantity more sensitive to the harmonic oscillation exhibited by the distribution, e.g. dividing the histogram into two hemispheres and looking at the difference in the event count. However, such an analysis would be intimately tied to the issue of disentangling the movement of the collider frame of reference with respect to the rest frame of  $\theta^{\mu\nu}$  from the measurement and therefore lies outside of the scope of this work.

## 6 Conclusions

We have studied the pair production of charged gauge bosons at the LHC in the NCSM. From the angular distributions in the decays of the gauge bosons we are able to partially reconstruct polarized cross sections. Using  $CP$  transformation properties we have constructed sensitive observable from suitable combinations of distributions. While the physics reach of the LHC remains at the TeraScale, these observables allow us to separate space-time from space-space noncommutativities.

## Acknowledgements

This research is supported by Bundesministerium für Bildung und Forschung Germany, grant 05HT6WWA and by the Helmholtz Alliance *Physics at the Terascale*. CS is supported by Deutsche Forschungsgemeinschaft through the Research Training Groups GRK 1147 *Theoretical Astrophysics and Particle Physics* and GRK 1102 *Physics of Hadron Accelerators*.

## A Feynman rules

### A.1 General Yang Mills theory

Collected in this section are the Feynman rules relevant for this work for a generic Yang Mills theory. As far as we know, they have not been previously presented in the literature. Feynman rules containing group generator matrices are to be understood as taking the matrix element corresponding to the combination of fermions meeting at the vertex. All momenta are ingoing. The covariant derivative is chosen as

$$D^\mu \Psi = \partial^\mu \Psi - ig A^\mu \Psi$$

The expansion of the lagrangian (4) to first order in  $\lambda$  yields the following correction to the vertex  $\bar{\Psi}\Psi A$

$$f, p, q, \bar{f}, q, A_i^\sigma = \frac{\lambda}{2} g T_i \theta^{\mu\nu\sigma} p_\mu q_\nu$$

with the totally antisymmetric symbol

$$\theta^{\mu\nu\sigma} = \theta^{\mu\nu} \gamma^\sigma + \theta^{\nu\sigma} \gamma^\mu + \theta^{\sigma\mu} \gamma^\nu$$

The vertex  $AAA$  receives the correction

$$A_i^\alpha, k_1, A_j^\beta, k_2, A_k^\gamma, k_3 = -\lambda g T_{i\{jk\}} \theta((k_1, \alpha), (k_2, \beta), (k_3, \gamma))$$

with the kinematic factor

$$\begin{aligned} \theta((k_1, \alpha), (k_2, \beta), (k_3, \gamma)) = & \\ & \theta_{\alpha\beta}((k_2 k_3) k_{1\gamma} - (k_1 k_3) k_{2\gamma}) + \\ & k_1 \theta_k(k_{3\beta} g_{\alpha\gamma} - k_{3\alpha} g_{\beta\gamma}) - \\ & k_1 \theta_\alpha(k_{2\gamma} k_{3\beta} - (k_2 k_3) g_{\beta\gamma}) + \\ & k_1 \theta_\beta(k_{2\gamma} k_{3\alpha} - (k_2 k_3) g_{\alpha\gamma}) + \\ & k_1 \theta_\gamma(k_{3\beta} k_{2\alpha} - (k_3 k_2) g_{\alpha\beta}) + \\ & \text{cycl. perm. of } ((\alpha, 1), (\beta, 2), (\gamma, 3)) \end{aligned}$$

and the representation dependent trace

$$T_{i\{jk\}} = \text{tr} T_i \{T_j, T_k\} = \frac{1}{3} \sum_{\text{perm}} T_i T_j T_k$$

A straightforward calculation shows that the vertex factor vanishes by contraction with one of the three momenta as required by gauge invariance.

(4) also gives rise to a new vertex  $\bar{\Psi}\Psi AA$

$$\begin{aligned} & \text{Diagram: } f \text{ (momentum } p) \text{ and } \bar{f} \text{ (momentum } q) \text{ meet at a vertex, with two outgoing wavy lines labeled } A_i^\rho \text{ (momentum } k_1) \text{ and } A_j^\sigma \text{ (momentum } k_2). \\ & = \\ & \frac{\lambda}{2} g^2 (p^\sigma \theta^{\sigma\rho} [T_i, T_j] + \\ & (k_1^\sigma \theta^{\sigma\rho} + p^\sigma \theta^\sigma \gamma^\rho + q^\sigma \theta^\rho \gamma^\sigma) T_i T_j + \\ & (k_2^\sigma \theta^{\sigma\rho} + p^\sigma \theta^\rho \gamma^\sigma + q^\sigma \theta^\sigma \gamma^\rho) T_j T_i + \\ & (k_1^\sigma \theta^\sigma \gamma^\rho + k_2^\sigma \theta^\rho \gamma^\sigma) \{T_i, T_j\}) \end{aligned}$$

## A.2 nmNCSM

From the general rules present above, the nmNCSM Feynman rules relevant for this work can be readily calculated by plugging in the nmNCSM fields, group representations and gauge couplings. While most of the following rules can already be found in [4], we repeat our result here because the  $f\bar{f}W^+W^-$  Feynman rule given in [4] applies only to the isospin up case, while the isospin down case turns out to be different. In appendix B we demonstrate that this variation is required by the corresponding Ward identities.

For all other rules, our calculation agrees with the results published in [4], and our isospin down  $f\bar{f}W^+W^-$  coupling also agrees with the Lagrangian given there (care must be taken in the

comparison as we give the rules for an ingoing fermion and an ingoing antifermion, while the authors of [4] chose an ingoing and an outgoing fermion).

$$\text{Diagram: } f \text{ (momentum } p) \text{ and } \bar{f} \text{ (momentum } q) \text{ meet at a vertex, with an outgoing wavy line labeled } A_\sigma. \\ = \frac{\lambda e}{2} Q p_\mu q_\nu \theta^{\mu\nu\sigma}$$

$$\begin{aligned} & \text{Diagram: } f_d, f_u \text{ (momentum } p) \text{ and } \bar{f}_u, \bar{f}_d \text{ (momentum } q) \text{ meet at a vertex, with an outgoing wavy line labeled } W_\sigma^\pm. \\ & = \\ & \frac{\lambda g}{2\sqrt{2}} p_\mu q_\nu \theta^{\mu\nu\sigma} \frac{1 - \gamma^5}{2} \end{aligned}$$

(where  $f_u$  resp.  $f_d$  denote a fermion with isospin up resp. down)

$$\begin{aligned} & \text{Diagram: } f \text{ (momentum } p) \text{ and } \bar{f} \text{ (momentum } q) \text{ meet at a vertex, with an outgoing wavy line labeled } Z_\sigma. \\ & = \\ & \frac{\lambda e}{2 \sin(2\theta_W)} p_\mu q_\nu \theta^{\mu\nu\rho} (g_V^f - g_A^f \gamma^5) \end{aligned}$$

with the vector and axial couplings

$$\begin{aligned} g_V^d &= \frac{2}{3} \sin^2(\theta_W) - \frac{1}{2} & g_A^d &= -\frac{1}{2} \\ g_V^u &= \frac{1}{2} - \frac{4}{3} \sin^2(\theta_W) & g_A^u &= \frac{1}{2} \\ g_V^l &= 2 \sin^2 \theta_W - \frac{1}{2} & g_A^l &= -\frac{1}{2} \\ g_V^\nu &= \frac{1}{2} & g_A^\nu &= \frac{1}{2} \end{aligned}$$

$$\begin{aligned} & \text{Diagram: } f_u \text{ (momentum } p) \text{ and } \bar{f}_u \text{ (momentum } q) \text{ meet at a vertex, with two outgoing wavy lines labeled } W_\rho^+ \text{ (momentum } k^+) \text{ and } W_\sigma^- \text{ (momentum } k^-). \\ & = \\ & \frac{g^2}{4} \theta^{\sigma\rho\mu} (k^+ + p)_\mu \frac{1 - \gamma^5}{2} \end{aligned}$$

$$f_d \xrightarrow{p} \text{---} \square \text{---} \begin{matrix} W_\rho^+ \\ k^+ \\ W_\sigma^- \\ k^- \end{matrix} = \frac{g^2}{4} \theta^{\sigma\rho\mu} (k^+ + q)_\mu \frac{1 - \gamma^5}{2}$$

$$A_\alpha \xrightarrow{k} \text{---} \square \text{---} \begin{matrix} W_\beta^+ \\ k^+ \\ W_\gamma^- \\ k^- \end{matrix} = -2eg^2 \kappa_2 \lambda \theta((k, \alpha), (k^+, \beta), (k^-, \gamma))$$

$$Z_\alpha \xrightarrow{k} \text{---} \square \text{---} \begin{matrix} W_\beta^+ \\ k^+ \\ W_\gamma^- \\ k^- \end{matrix} = 2egg' \kappa_2 \lambda \theta((k, \alpha), (k^+, \beta), (k^-, \gamma))$$

## B Ward identities for $u\bar{u} \longrightarrow W^+W^-$ and $d\bar{d} \longrightarrow W^+W^-$

We demonstrate the necessity of amending the Feynman rules of [4] as in appendix A.2 by verifying the corresponding Ward identity in the limit of vanishing gauge boson masses:

$$k_\mu^+ \epsilon_\nu^- \mathcal{M}^{\mu\nu}(q\bar{q} \rightarrow W^+W^-) = 0. \quad (16)$$

Since the full  $\mathbf{SU}(1)_L \times \mathbf{U}(1)_Y$  symmetry is restored in this limit, we can simplify the calculation by using the gauge eigenstate  $W_3$  instead of  $A$  and  $Z$  in the  $s$  channel. Also note that the  $s$ -channel diagram with a NC insertion for the triple gauge boson vertex depends on the representation chosen in the gauge sector and therefore satisfies the Ward identity individually.

We are left with the following four diagrams:

$$u/d \xrightarrow{p} \text{---} \square \text{---} \begin{matrix} W^- \\ k^- \\ W^+ \\ k^+ \end{matrix} = i\mathcal{M}_{u\bar{u}/d\bar{d},s}^{\mu\nu} k_\mu^+ \epsilon_\nu^-$$

$$u/d \xrightarrow{p} \text{---} \square \text{---} \begin{matrix} W^-/+ \\ k^-/+ \\ W^+/- \\ k^+/- \end{matrix} = i\mathcal{M}_{u\bar{u}/d\bar{d},t,-/+}^{\mu\nu} k_\mu^+ \epsilon_\nu^-$$

$$u/d \xrightarrow{p} \text{---} \square \text{---} \begin{matrix} W^-/+ \\ k^-/+ \\ W^+/- \\ k^+/- \end{matrix} = i\mathcal{M}_{u\bar{u}/d\bar{d},t,+/ -}^{\mu\nu} k_\mu^+ \epsilon_\nu^-$$

$$u/d \xrightarrow{p} \text{---} \square \text{---} \begin{matrix} W^- \\ k^- \\ W^+ \\ k^+ \end{matrix} = i\mathcal{M}_{u\bar{u}/d\bar{d},4}^{\mu\nu} k_\mu^+ \epsilon_\nu^-.$$

Since the choice of incoming vs. outgoing momenta and particle vs. antiparticle is of crucial importance for our argument, we elect to compute the crossed amplitude with *all* particles, momenta and quantum numbers *incoming*, as this offers the least possibility for confusion when applying the Feynman rules. While this amplitude does not correspond to a physical process, it is related to one by crossing symmetry and must therefore satisfy the Ward identity (16) as well.

Using the Feynman rules of appendix A.2 and extracting common coupling factors and external fermion wave functions

$$\mathcal{M}_i^{\mu\nu} k_\mu^+ \epsilon_\nu^- = \lambda \frac{g^2}{4} \bar{v}(q) \Gamma_i \frac{1 - \gamma^5}{2} u(p) \quad (17)$$

we find for the individual contributions

$$\Gamma_{u\bar{u},s} = (q\theta p)\not{\epsilon}_- \quad (18a)$$

$$\Gamma_{d\bar{d},s} = (p\theta q)\not{\epsilon}_- \quad (18b)$$

$$\Gamma_{u\bar{u},t,-} = (k_-\theta p)\not{\epsilon}_- - (\epsilon_-\theta p)\not{k}_- \quad (18c)$$

$$\Gamma_{d\bar{d},t,-} = (k_-\theta q)\not{\epsilon}_- - (\epsilon_-\theta q)\not{k}_- \quad (18d)$$

$$\Gamma_{u\bar{u},t,+} = 0 \quad (18e)$$

$$\Gamma_{d\bar{d},t,+} = 0 \quad (18f)$$

$$\Gamma_{u\bar{u},4} = (k_+\theta p)\not{\epsilon}_- - (\epsilon_-\theta p)\not{k}_+ \quad (18g)$$

$$\Gamma_{d\bar{d},4} = (k_+\theta q)\not{\epsilon}_- - (\epsilon_-\theta q)\not{k}_+ \quad (18h)$$

after using momentum conservation, mass shell conditions, transversality and the Dirac equations

$$p + q + k^+ + k^- = 0 \quad (19a)$$

$$p^2 = q^2 = k^{+2} = k^{-2} = 0 \quad (19b)$$

$$k^- \epsilon^- = 0 \quad (19c)$$

$$\not{p}u(p) = 0 \quad (19d)$$

$$\bar{v}(q)\not{q} = 0 \quad (19e)$$

repeatedly. Using (19) again, we can verify from (18) the Ward identities in both cases

$$\Gamma_{u\bar{u},s} + \Gamma_{u\bar{u},t,-} + \Gamma_{u\bar{u},t,+} + \Gamma_{u\bar{u},4} = 0 \quad (20a)$$

$$\Gamma_{d\bar{d},s} + \Gamma_{d\bar{d},t,-} + \Gamma_{d\bar{d},t,+} + \Gamma_{d\bar{d},4} = 0. \quad (20b)$$

However we also see that the individual contributions differ, in particular

$$\Gamma_{u\bar{u},4} \neq \Gamma_{d\bar{d},4}, \quad (21)$$

even if the relations (19) are taken into account.

This completes our proof that the different momentum dependence of the quartic couplings for quarks with isospin up and down, as obtained from the Lagrangian in [4] but missing from the Feynman rules given in the same publication, is required by gauge invariance. It has to cancel unphysical contributions that have a different momentum dependence, because charge conservation exchanges a  $t$ -channel diagram in  $\mathcal{M}_{u\bar{u},t,-}^{\mu\nu}$  by a  $u$ -channel diagram in  $\mathcal{M}_{d\bar{d},t,-}^{\mu\nu}$ .

## References

- [1] N. Seiberg and E. Witten, JHEP **9909**, 032 (1999) [arXiv:hep-th/9908142].
- [2] J. Madore, S. Schraml, P. Schupp and J. Wess, Eur. Phys. J. C **16**, 161 (2000) [arXiv:hep-th/0001203]; B. Jurco, L. Moller, S. Schraml, P. Schupp and J. Wess, Eur. Phys. J. C **21**, 383 (2001) [arXiv:hep-th/0104153].
- [3] X. Calmet, B. Jurco, P. Schupp, J. Wess and M. Wohlgenannt, Eur. Phys. J. C **23**, 363 (2002) [arXiv:hep-ph/0111115].
- [4] B. Melic, K. Passek-Kumericki, J. Trampetic, P. Schupp and M. Wohlgenannt, Eur. Phys. J. C **42**, 483 (2005) [arXiv:hep-ph/0502249]; Eur. Phys. J. C **42**, 499 (2005) [arXiv:hep-ph/0503064].
- [5] A. Alboteanu, T. Ohl and R. Rückl, Phys. Rev. D **74**, 096004 (2006) [arXiv:hep-ph/0608155].
- [6] I. Hinchliffe, N. Kersting and Y. L. Ma, Int. J. Mod. Phys. A **19**, 179 (2004) [arXiv:hep-ph/0205040].
- [7] W. Behr, N. G. Deshpande, G. Duplancic, P. Schupp, J. Trampetic and J. Wess, Eur. Phys. J. C **29**, 441 (2003) [arXiv:hep-ph/0202121].
- [8] T. Ohl and J. Reuter, Phys. Rev. D **70** (2004) 076007 [arXiv:hep-ph/0406098].
- [9] W. Kilian, T. Ohl and J. Reuter, arXiv:0708.4233 [hep-ph].
- [10] T. Asakawa and I. Kishimoto, JHEP **9911**, 024 (1999) [arXiv:hep-th/9909139].
- [11] P. Aschieri, B. Jurco, P. Schupp and J. Wess, Nucl. Phys. B **651**, 45 (2003) [arXiv:hep-th/0205214].
- [12] A. Alboteanu, T. Ohl and R. Rückl, Phys. Rev. D **76** (2007) 105018 [arXiv:0707.3595 [hep-ph]].
- [13] M. M. Sheikh-Jabbari, Phys. Rev. Lett. **84**, 5265 (2000) [arXiv:hep-th/0001167].
- [14] J. A. M. Vermaseren, [arXiv:math-ph/0010025].
- [15] M. Moretti, T. Ohl and J. Reuter, [arXiv:hep-ph/0102195].

- [16] H. L. Lai *et al.* [CTEQ Collaboration], Eur. Phys. J. C **12**, 375 (2000) [arXiv:hep-ph/9903282].
- [17] J. A. Conley and J. L. Hewett, [arXiv:0811.4218 [hep-ph]].
- [18] T. Ohl and C. Speckner, Phys. Rev. D **78** (2008) 095008 [arXiv:0809.0023 [hep-ph]].
- [19] E. Boos and T. Ohl, Phys. Rev. Lett. **83** (1999) 480 [arXiv:hep-ph/9903357]; T. Ohl and C. Schwinn, Eur. Phys. J. C **30**, 567 (2003) [arXiv:hep-ph/0305334].